PREDICTION OF GAS OUTBURST IN A COAL MINE BASED ON SIMULTANEOUS PRESTACK SEISMIC INVERSION: A CASE STUDY IN CHINA

JUANJUAN LI[1,2], RUOFEI CUI[1], DONGMING PAN[1], SHENEN CHEN[1], MINGSHUN HU[1] and XIN ZHAO[3]

[1] *China University of Mining and Technology, Xuzhou 221116, P.R. China.*
[2] *Department of Civil Engineering, University of North Carolina at Charlotte, Charlotte, NC 28223, U.S.A. lijuanjuan1985@gmail.com*
[3] *IoT Perception Mine Research Center, China University of Mining and Technology, Xuzhou 221118, P.R. China.*

(Received May 19, 2013; revised version accepted September 2, 2013)

ABSTRACT

Li, J., Cui, R., Pan, D., Chen, S., Hu, M. and Zhao, X., 2013. Prediction of gas outburst in a coal mine based on simultaneous prestack seismic inversion: a case study in China. *Journal of Seismic Exploration*, 22: 453-475.

In deep mines, gas outburst accidents can result in serious coal mine safety and economic loss, which means extraction of coal from the deep strata can be a critical problem for industry energy in China. Based on the differences in the physical properties between deformed coal and original bituminous coal, this paper shows the results in different seismic attributes: acoustic impedance, elastic impedance, $\mu*\rho$ and $\lambda*\rho$ from prestack seismic data, and suggest that they can be used to assess the distribution of deformed coal. Our results show that the gas outburst associated with the distribution of deformed coal can be reliably predicted. We conclude that the prestack seismic attributes provide a new way of effectively assessing potential risks of gas outburst in mining operation, and may therefore be practically used in the large-scale development of coal bed methane resources.

KEY WORDS: deformed coal, elastic impedance inversion, simultaneous inversion, gas outburst prediction.

INTRODUCTION

Coal is the major source of energy in China, which accounts for about 70% of the total energy production. It is predicted that coal-based energy structure will not likely change at least for the next 50 years. As mining operations get deep and deeper, coal mining related geological disasters become more prominent.

0963-0651/13/$5.00

Mining-related disasters, for example, have brought huge losses to the Chinese economy and has resulted in a serious threat to the safety of miners. In China, coal production accounts for about 37% of the world's total, but the death total is about 70% of the worldwide coal mine death toll. The gas outburst accidents cover 70% of major disasters. Hence, also referred as "the first killer". There have been more than 15,000 incidents since the first gas outburst was recorded in the 1950's in China. 270 mines have had gas accidents, most of which are results from shallow depths of less than 75 m. The most significant accident was reported in the Da-Ping mine, where 148 died on October 20, 2004. There is an immediate need to study the occurrence of mine and gas outbursts and to provide better geological understanding and reliable method to predict those accidents for safe coal production (He, 1999; Cheng and Zhang, 2005; Zhou, 1999; Yu, 1993).

A variety of methods to predict gas outburst accident have been proposed, after the Isaac mine of the Ruhr coalfield gas accident on March 22, 1834 in France, which was recorded as the first gas outburst accident in the history of mankind. Many studies have shown that the area, where coal and gas outbursts occur, definitely has a certain presence of deformed coal. The existence of deformed coal is not always the condition but a requirement for the gas outburst to occur. Hence it is necessary to study deformed coal distribution and the relationship between gas outburst and deformed coal development.

CHARACTERISTICS OF DEFORMED COAL

Deformed coal is formed by bituminous coal, due to tectonic movement, that crushes it into particles, flakes or powder. As a results of strong brittle or ductile deformation, coal gets damaged and the rock mass gets fractured. Deformed coal is different in the following ways: Deformed coal density is generally lower than that of the original bituminous coal, and pore space (including both mesoscopic pores and microscopic pore volumes) is increased during the evolution. Due to its flaky or powdery structure, the propagation velocity of waves in deformed coal gets smaller. Strength coefficient of deformed coal, depending on the extent of the damage, are generally smaller than the original bituminous. The crushing also causes changes in the electrochemical natures, and the resistivity of the coal decreases with increase in the extent of fragmentation.

According to both the macro-structural and micro-structural features of coal, coal is divided into four types: original bituminous coal, fragmentation coal, crushed coal and mylonitic coal (He, 1999). The relationship between types of coal and gas outburst can be summarized as follows: (1) gas outburst is closely related to the tectonic movement which the coal seams experienced; (2) gas outburst accidents are most unlikely without the destructive tectonic

movement; and (3) positive correlation: the extent of the damage is that the higher the damage, the more likely a gas outburst could occur.

PRESTACK SEISMIC INVERSION

Acoustic Impedance (AI) is a seismic attribute that can be used for lithological and fluid prediction. It was first proposed in the 1970's and has become very popular since the 1990's. Connolly (1999) proposed the concept of Elastic Impedance (EI), which is a function of P-wave velocity, S-wave velocity and angle of incidence. EI has been shown to better detect fluid and lithology than AI. Whitcombe (2002a, 2002b) further improved the EI equation, and proposed the Extended Elastic Impedance (EEI). Following Connolly's EI equation, the prestack AVA (Amplitude Versus Angle) simultaneous was proposed (Hampson et al., 2005; Li, et al., 2007), where upon P-wave S-wave velocity and density can be the calculated from angle stacks, and the method also enriches lithology and fluid identification means.

Peng et al. (2005) gave an example of detecting coal cleat fissures and predicting coalbed methane distribution using the AVO technique. Xu (2008) applied the poststack inversion techniques in thin coal seam morphology and complex tectonic lithological interpretation. Sun (2010) attempted to detect deformed coal distribution using the prestack inversion techniques and probabilistic neural network (PNN) technique to obtain structural transition to lithological exploration in coalfield.

Prestack inversion is based on the Zoeppritz's equation (Aki and Richard, 1980; Sheuy, 1985). Both EI inversion and simultaneous inversion techniques belong to prestack inversion - EI inversion based on Shuey's equation, while simultaneous inversion originated in the Aki-Richard equation.

Elastic impedance inversion

Shuey (1985) studied the impact of Poisson's ratio on the variation of P-wave reflection coefficient with incident angle θ, and proposed the simplified equation for the Zeoppritz equation,

$$R/R_0 \approx 1 + A\sin^2\theta + B(\tan^2\theta - \sin^2\theta) \quad , \tag{1}$$

where we have defined

$$R_0 \approx \tfrac{1}{2}[(\Delta v_P/v_P) + (\Delta\rho/\rho)] \ , \ A = A_0 + [1/(1-\sigma)^2 * (\Delta\sigma/R_0)] \ ,$$

$$B = (\Delta v_P/v_P)/[(\Delta v_P/v_P) + (\Delta\rho/\rho)] \ , \ A_0 = B - 2(1+B)[(1-2\sigma)/(1-\sigma)].$$

For normal incidence (zero degree incident angle), the reflection coefficient can be expressed as,

$$R = (\rho_2 v_2 - \rho_1 v_1)/(\rho_2 v_2 + \rho_1 v_1)$$

$$= (AI_2 - AI_1)/(AI_2 + AI_1) \approx \tfrac{1}{2}\Delta \ln AI \ , \quad (2)$$

For non-normal incidence, Connolly (1999) proposed the following reflection coefficient in the same form as for normal incidence in eq. (2),

$$R = (EI_2 - EI_1)/(EI_2 + EI_1) \approx \tfrac{1}{2}\Delta \ln EI \ . \quad (3)$$

Shuey's (1995) equation can be expanded to,

$$R = \tfrac{1}{2}[(\Delta v_P/v_P) + (\Delta\rho/\rho)]$$

$$+ [(\Delta v_P/v_P) - 4(v_S^2/v_P^2)(\Delta v_S/v_S) - 2(v_S^2/v_P^2)(\Delta\rho/\rho)]\sin^2\theta$$

$$+ \tfrac{1}{2}(\Delta v_P/v_P)\sin^2\theta\tan^2\theta$$

$$= \tfrac{1}{2}\{(\Delta v_P/v_P)(1 + \tan^2\theta) - 8(\Delta v_S/v_S)(v_S^2/v_P^2)\sin^2\theta$$

$$+ (\Delta\rho/\rho)[1 - 4(v_S^2/v_P^2)\sin^2\theta]\}$$

$$= \tfrac{1}{2}\Delta \ln(v_P^{(+\tan^2\theta)} v_S^{[-8(v_S^2/v_P^2)\sin^2\theta]} \rho^{[1-4(v_S^2/v_P^2)\sin^2\theta]}) \ . \quad (4)$$

According to the equations (3) and (4), elastic impedance EI can be expressed as (Connolly, 1999; Pan et al., 2006),

$$EI = v_P^{(+\tan^2\theta)} v_S^{[-8(v_S^2/v_P^2)\sin^2\theta]} \rho^{[1-4(v_S^2/v_P^2)\sin^2\theta]} \ . \quad (5)$$

For 0° incidence angle, EI value equals AI value. Because of the same form of normal incident and non-normal incidence, any existing poststack inversion technique can be applied to calculate the prestack elastic impedance inversion.

Simultaneous inversion

Simultaneous inversion of prestack seismic data is an effective method to identify lithology and fluid (Hampson et al., 2005; Li et al., 2007). The logarithm value of P-wave impedance and S-wave impedance has been shown to have a linear relationship, and the Aki-Richard's equation can therefore be approximated by the expression of the relationship between P-wave reflection coefficients and angle of reflection - these are prerequisites established by the simultaneous inversion technique.

The linear correlations of P-wave impedance and S-wave impedance can be generally expressed as follows,

$$\ln(\rho) = m\ln(Z_P) + m_c + \Delta L_D \quad , \tag{6}$$

and

$$\ln(Z_S) = k\ln(Z_P) + k_c + \Delta L_S \quad . \tag{7}$$

The simultaneous inversion is based on re-group of the Aki-Richard approximation and the derivation is given below,

$$R_P(\theta) = C_1 R_P + C_2 R_S + C_3 R_d \quad , \tag{8}$$

where $C_1 = 1 + \tan^2\theta$, $C_2 = -8\gamma^2\sin^2\theta$, $C_3 = 2\gamma^2\sin^2\theta - 0.5\tan^2\theta$, $L_S = \ln Z_S$, $L_d = \ln Z_d$ and $L_P = \ln Z_P$. The subscript d represents the differential matrix,

$$R_P = \tfrac{1}{2}DL_P \quad , \quad R_S = \tfrac{1}{2}DL_S \quad , \quad R_d = \tfrac{1}{2}DL_d \quad .$$

The Aki-Richard approximation is then transformed into the following,

$$R_P = (C_1/2)DL_P + (C_2/2)DL_S + C_3 DL_d \quad . \tag{9}$$

Eq. (9) can also be expressed as,

$$T(\theta) = W(\theta) * R_P(\theta) \quad , \tag{10}$$

where $T(\theta)$ represents the angle gathers or angle stacks and $W(\theta)$ represents the wavelets associated with angle gathers. Substituting eq. (9) into eq. (10), we obtain

$$T(\theta) = (C_1/2)W(\theta)DL_P + (C_2/2)W(\theta)DL_S + C_3 W(\theta)DL_d \quad . \tag{11}$$

Eq. (11) is the basis of simultaneous inversion. The number of prestack angle stacks involved in the simultaneous inversion is generally greater than 3 (we use 5 angle stacks in this paper), so the equation is over-determined and can be solved by the conjugate gradient method.

CASE STUDY

During the mining process in the Xinjing coal mine, many gas outburst accidents have been reported. So the mine has been identified as the gas outburst mine. In this study, the prestack lithology inversion is used to determine areal distributions of potential gas outbursts.

Coal seam occurrence

Coal-bearing strata is a combination of the upper Carboniferous Taiyuan group formation and the lower Permian Shanxi group formation. The average thickness of the coal-bearing strata is 177.68 m with total coal seam thickness 20.85 m (the coal-bearing coefficient is 11.73%). The average thickness of the Taiyuan formation is 120.88 m, with 9-layer coal seams. The number 15 coal seam (including mergers layer) is a stable and mineable layer, the numbers 8, 9 and lower coal of number 15 under coal seams are relatively stable and probable mineable layer, the numbers 12 and 13 are unstable and locally mineable while the upper seam of numbers 8 and 9, the number 11 are unstable and sporadic mineable coal seams. Average total thickness of the coal seam is 15.57 m and the coal-bearing coefficient is 12.88%. The average thickness of the Shanxi formation is 56.8 m, with 6-layer coal seams. The number 3 coal seam is a stable and mineable coal layer, six coal-bearing layers are unstable and local mineable while numbers 1, 2, 4, and 5 and are unstable and sporadic mineable or un-mineable coal seams. Average total thickness of the coal seam is 5.28 m and the coal-bearing coefficient is 9.30%.

A local research institute (Chongqing Coal Academy) has evaluated the gas classification in the Yang-Quan coal mine in November 2006 and reported that the absolute gas emission is 212.6212.6 m^3/min; the relatively gas emission is 21.35 m^3/t; the maximum relative emission is 106.3 m^3/t; the absolute carbon dioxide emission is 5.79 m^3/min and the relative carbon dioxide emission 0.58 m^3/t. So this coal mine is determined to be a mine with potential gas outburst. In the paper, we will study the distribution of deformed coal and evaluate the possibility of gas outburst in the number 15 coal seam.

Elastic impedance inversion application

In the seismic data processing, we have included a surface consistent processing, spread wavefront compensation and linear interference removal to improve the data processing effects and preserve relative amplitudes that are required for prestack inversion. Five angle stacks (7°, 10°, 13°, 16°, and 19°) are extracted and one inline angle stack is shown in Fig. 1.

In contrast to AI, EI has a better lithological discrimination and fluid identification because EI does not rely on the assumption of normal incidence. We have applied both AI and EI inversions and the values of AI and EI results are normalized to be between 0 and 1 for the purpose of comparison.

AI and EI inversion results of one inline profile are shown in Fig. 2, which shows that EI inversion has a slightly better event or lithology continuity

than AI in the seam roof and floor marked by ellipses. The EI and AI sections extracted from the impedance inversion data along the lowest trend in the seam are shown in Fig. 3, where Fig. 3 (Left) is the AI inversion results and Fig. 3 (Right) is the EI inversion results. Green and yellow colours represent small wave impedance value while red, blue and purple colours represent large values. The EI section is more sensitive to the high impedance layer and the high impedance boundaries are more clearly identified, as is shown by the black polygons in Fig. 3.

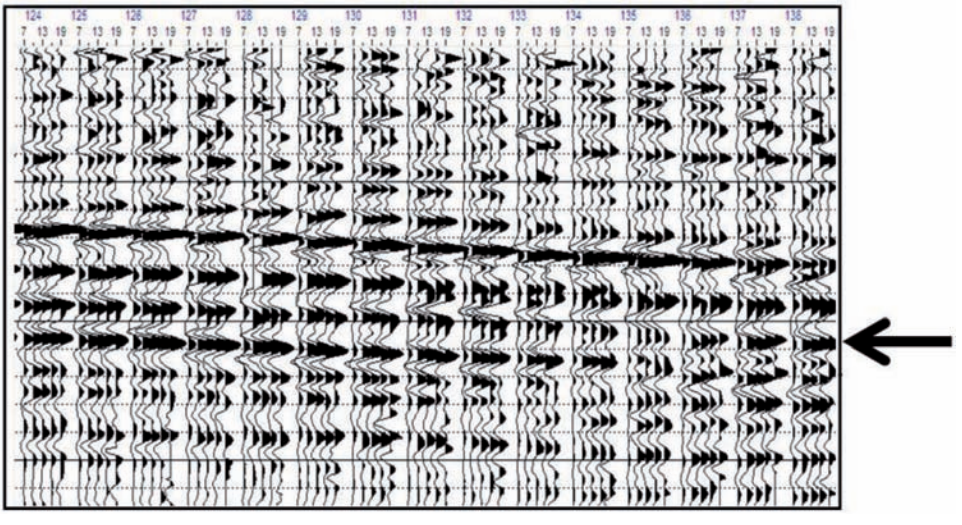

Fig. 1. Angle gathers of an inline in the coal mine. The arrow marked the target coal seam (number 15).

Deformed coal has the characteristics of low impedance in both EI and AI results. Especially EI is theoretically of lower value (Sun, 2011). CMP points of EI impedance value ($\leq$ 0.17) and AI impedance value ($\leq$ 0.2) are respectively projected onto the plan along the number 15 coal seam inversion section as shown in Fig. 4. The CMP points (EI value $<$ AI value) are projected as shown in Fig. 5. Based on the inversion results, the deformed coal distribution are predicted and delineated as marked by the black polygons.

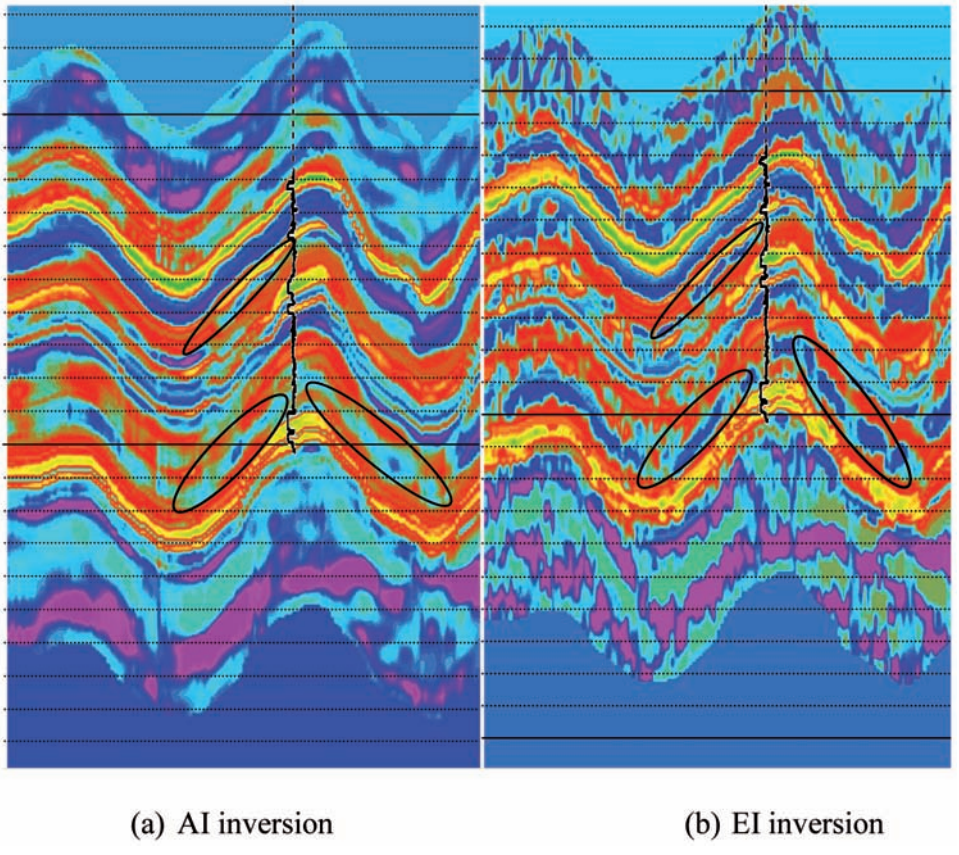

Fig. 2. An inline profile of AI and EI inversion result. (Left) AI inversion; (Right) EI inversion.

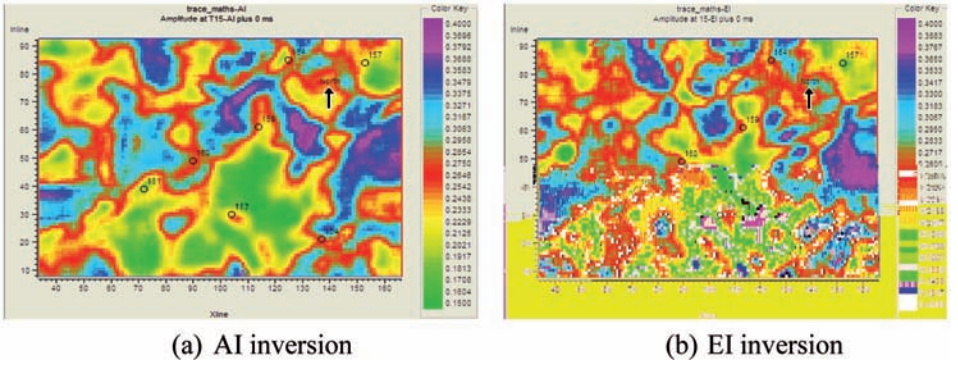

Fig. 3. AI and EI inversion slices. (Left) AI inversion; (Right) EI inversion.

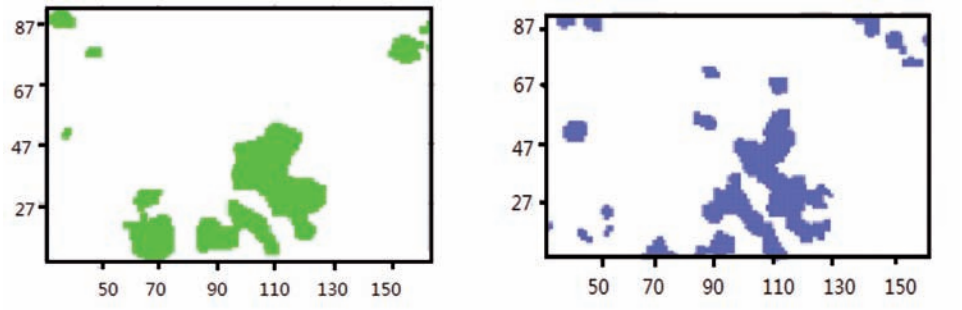

Fig. 4. EI value ($\leq$ 0.17) and the AI value ($\leq$ 0.2) CMP projection plan. (Left) AI value ($\leq$ 0.2) CMP projection plan; (Right) EI value ($\leq$ 0.15) CMP projection plan.

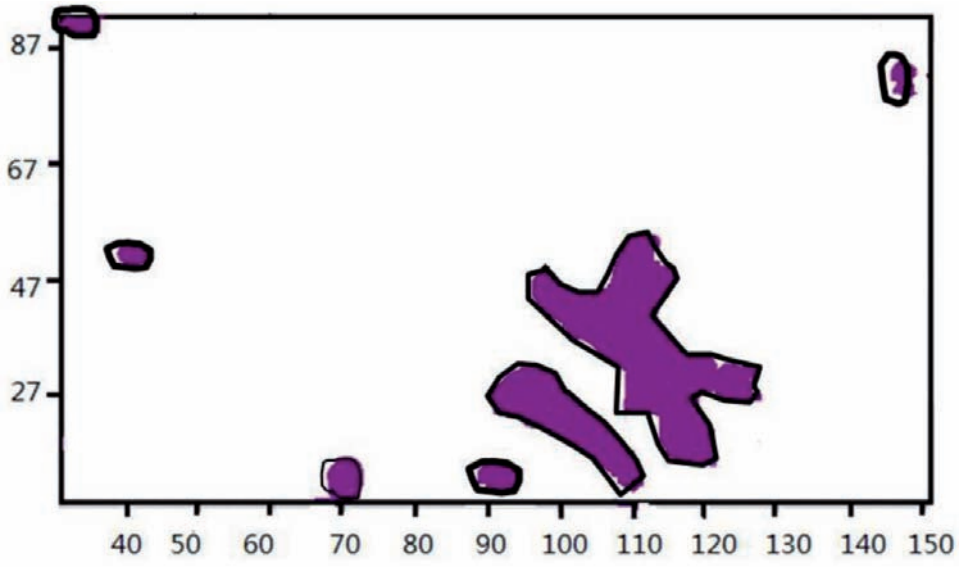

Fig. 5. CMP (EI < AI) projection plan.

Simultaneous inversion application

In this section, we show the results of deformed coal distribution from the simultaneous inversion in the form of $\lambda * \rho$ and $\mu * \rho$ attributes. The number 15 coal seam attribute sections are generated along the lowest trend in the $\lambda * \rho$ and $\mu * \rho$ volumes in Fig. 6.

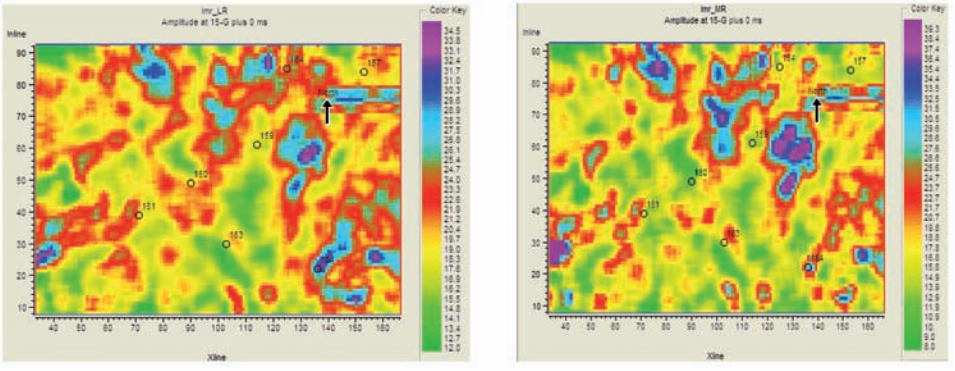

(a) $\lambda * \rho$ slice (b) $\mu * \rho$ slice

Fig. 6. $\lambda * \rho$ and $\mu * \rho$ slices along the coal seam. (Left) $\lambda * \rho$ slice; (Right) $\mu * \rho$ slice.

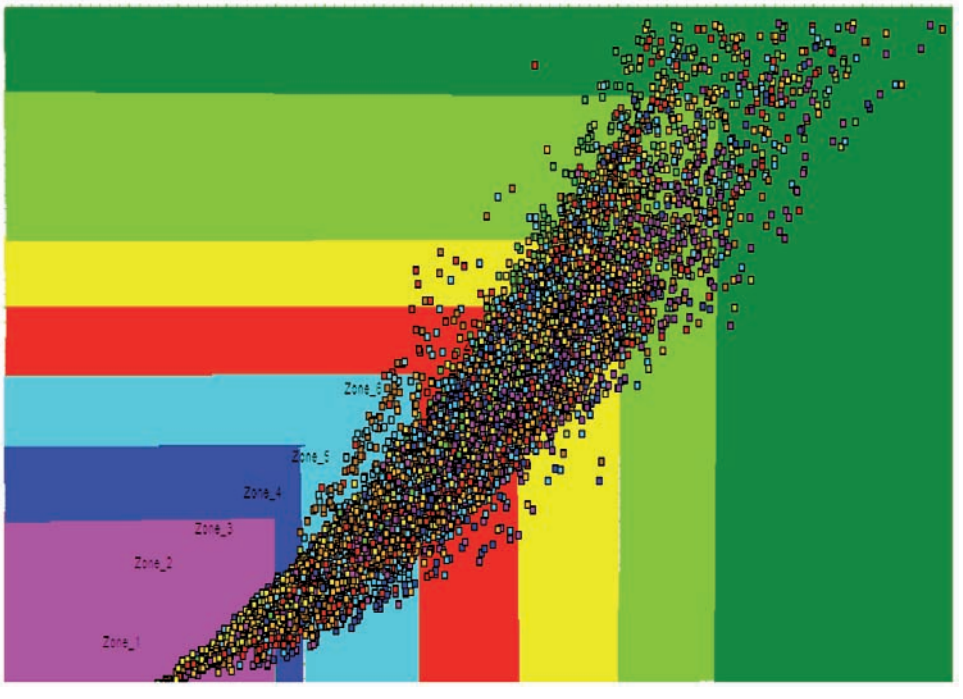

Fig. 7. $\lambda * \rho$ and $\mu * \rho$ zoning map along the 15 coal seam slice.

The criterion of identification deformed coal is given as $\lambda * \rho \leq 12$ and $\mu * \rho \leq 8$. The crossplot of $\lambda * \rho$ and $\mu * \rho$ data is made to identify areal distribution of deformed coal in the number 15 coal seam. Then 7 zones are divided in the crossplot and the purple rectangle represents the deformed coal shown in Fig. 7.

The crossplot zoning is applied to the attribute data, and then we pick the deformed coal zone along the number 15 coal seam and project CMP in Fig. 8. Finally we delineate A.B.C.D.E.F and G areas of low $\lambda * \rho$ and $\mu * \rho$ values with the red polygons as deformed coal distributions. To better explain the abnormal distribution and verify the effectiveness of the simultaneous and EI inversions, the results are compared in Fig. 8, where deformed coal distribution from the EI inversion is marked by black polygons. Both results from EI and simultaneous inversions are basically consistent - the result of D and E areas with large range abnormal are reliable; the result of A, C and G areas with small abnormal is relatively reliable; the result of B and F areas is unreliable as the EI result is inconsistent with the simultaneous inversion. Based on our interpretation of the deformed coal distribution, we may conclude that the gas outburst is more likely to occur in the D and E areas, while less likely in the A, C and G areas and least likely in B and F areas.

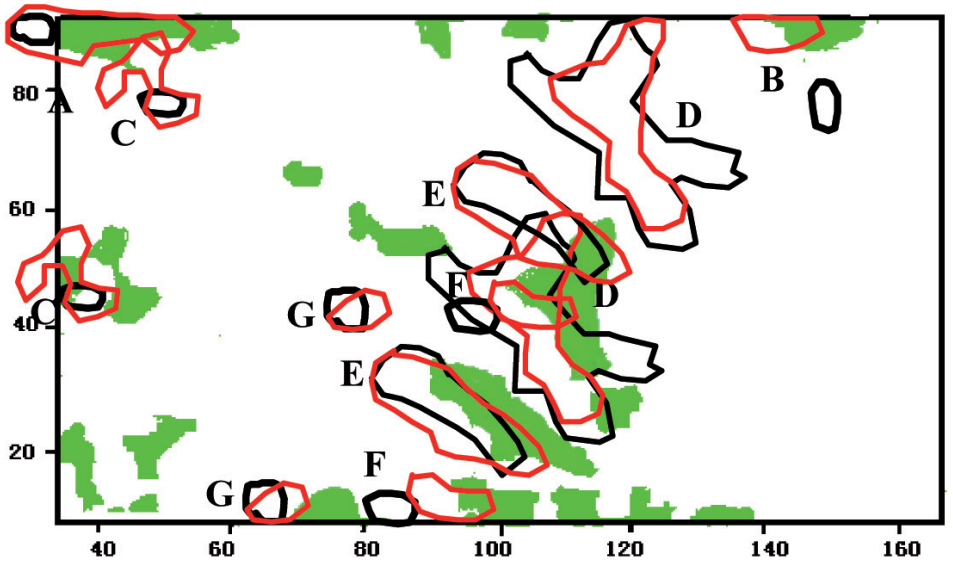

Fig. 8. CMP projection of deformed coal zone slice.

CONCLUSIONS

In this paper, we have identified the deformed coal distribution and potential gas outburst areas in the number 15 coal seam in the Xingjing coal mine of Yangquan using prestack lithology inversion. Deformed coal's physical properties are different in many ways compared to the original bituminous coal lower density, lower velocity, smaller elastic coefficient. These differences form the physical basis for the identification of deformed coal seam distribution (therefore potential gas outburst locations). The EI inversion, based on Zeoppritz approximate equation, has a better lithology discrimination than the AI inversion. The EI result of the number 15 coal seam was compared with the AI result. We have also generated $\lambda * \rho$ and $\mu * \rho$ using prestack simultaneous inversion. 7 deformed coal distribution areas have been classified, among which 2 abnormal large ranges can be interpreted as reliable deformed coal development regions, therefore potential gas outburst locations. Our results are currently used by the local authority in the risk assessment of mining safety.

EI, $\lambda * \rho$ and $\mu * \rho$ of deformed coal are characterized by a low-value, and therefore can be used identify potential gas outburst locations. The relationship between distribution of deformed coal and coal seam gas outburst can be reliably used to evaluate the possibility of gas outburst. Gas outburst is an extremely complex geological phenomenon involved with many factors. The roof lithology is one of the important factors affecting gas outburst. In general mudstone capping type is easy to confine gas and sandstone capping is poor to confine gas. Different seismic attributes can be used to predict the lithological distribution surrounding coal-bearing layers and therefore used to assess the potential risk of gas outbursts in mining operation.

ACKNOWLEDGEMENT

The authors acknowledge the financial support from: the CBM exploration three-dimensional inverse VSP technology research (2011ZX05035-003-002HZ), National Key Basic Research and Development Program (973) (2007CB209400, 2009CB219603), National Natural Foundation of China (40874054) and Fundamental Research of the Central Universities of Special Funds item (2010ZDP01A07), and the China Scholarship Council.

REFERENCES

Aki, K. and Richards, P.G., 1980. Quantitative Seismology. W.H. Freeman and Co., San Francisco.

Cheng, W. and Zhang, X., 2005. Coal and Gas Outburst Prediction: Theory and Technology. Coal Industry Press, Beijing.

Connolly, P., 1999. Elastic impedance. The Leading Edge, 18: 438-452.

Hampson, D.P., Russell, B.H. and Bankhead, B., 2005. Simultaneous inversion of prestack seismic data. Expanded Abstr., 75th Ann. Internat. SEG Mtg., Houston: 1633-1637.

He, J., 1999. The Gas Outburst Geophysical Research. Central South University Press, Changsha (China).

Li, A., Yin, X. and Zhang, F., 2007. Prestack AVA multi-parameter simultaneous inversion in the prediction of gas-bearing reservoirs application. Petrol. Explor., 46: 64-68.

Pan, D.M., Liu, E. and Yue, J.H., 2006. Comparison of the accuracies of elastic impedance. J. Seismic Explor., 15: 303-317.

Peng, S., Gao, Y. and Yang, R., 2005. Theory and application of AVO for detection of coalbed methane - A case from the Huainan coalfield. Petrol. Explor., 48: 1475-1486.

Richard, P.J. and Frasier, C.W., 1976. Scattering of elastic waves from depth-dependent inhomogeneities. Geophysics, 41: 441-458.

Sun, X., 2011. Lithological parameters prestack inversion methods of coal reservoirs. China University of Mining and Technology: 69-71.

Shuey, A., 1985. Simplification of the Zoeppritz equations. Geophysics, 50: 609-614.

Whitcombe, D.N, 2002. Elastic impedance normalization. Geophysics, 67: 60-62.

Whitcombe, D.N., 2002. Extended elastic impedance for fluid and lithology. Geophysics, 67: 63-67.

Yu, Q., 1993. Mine Gas Prevention and Control. China University of Mining and Technology Press, Xuzhou (China).

Zhou, S., 1999. Coalseam Gas Occurrence Flow Theory. Coal Industry Press, Beijing (China).